Detecting large-scale networks in the human brain using high-density electroencephalography

Quanying Liu[1,2,3], Seyedehrezvan Farahibozorg[3,4], Camillo Porcaro[2,5,6],

Nicole Wenderoth[1,2], Dante Mantini[1,2,3]

[1] Neural Control of Movement Laboratory, ETH Zurich, 8057 Zurich, Switzerland;

[2] Laboratory of Movement Control and Neuroplasticity, KU Leuven, 3001 Leuven, Belgium;

[3] Department of Experimental Psychology, Oxford University, Oxford OX1 3UD, United Kingdom;

[4] MRC Cognition and Brain Sciences Unit, Cambridge CB2 7EF, United Kingdom;

[5] LET'S-ISTC-CNR, Fatebenefratelli Hospital, 00186 Rome, Italy;

[6] Department of Information Engineering, Marche Polytechnic University, 60131 Ancona, Italy.

Corresponding author:

Dr. Dante Mantini

Department of Health Sciences and Technology, ETH Zurich

Winterthurerstrasse 190, 8057 Zurich, Switzerland

Telephone: +41 44 632 42 01

Fax: +41 44 632 42 56

Email: dante.mantini@hest.ethz.ch

Running title: Imaging brain networks with high density EEG

Abstract

High-density electroencephalography (hdEEG) is an emerging brain imaging technique that can permit investigating fast dynamics of cortical electrical activity in the healthy and the diseased human brain. Its applications are however currently limited by a number of methodological issues, among which the difficulty in obtaining accurate source localizations. In particular, these issues have so far prevented EEG studies from showing brain networks similar to those previously detected by functional magnetic resonance imaging (fMRI). Here, we report for the first time a robust detection of brain networks from resting state (256-channel) hdEEG recordings, with a spatial accuracy comparable to fMRI networks. This result was achieved by setting up a tailored analysis pipeline including state-of-the-art tools for data preprocessing, realistic head model generation, source localization and functional connectivity analysis. Specifically, we obtained the highest similarity between hdEEG and fMRI networks by means of realistic 12-layer head models and eLORETA source localization, together with spatial ICA for functional connectivity analysis. Spatial ICA overcomes the spatial leakage problem by identifying patterns of coherent power fluctuations that are spatially independent over time. Our analyses showed that the number of electrodes in particular, but also the accuracy of the head model and the source localization method used have impact on network reconstruction. We believe that our methodological work can contribute to rise of hdEEG as a powerful tool for brain research.

Keywords: electroencephalography; high-density montage; resting state network; functional connectivity; neuronal communication

1. Introduction

Physiological, neuropsychological and neuroimaging studies have clearly revealed that functional specialization and integration are two distinct, yet coexisting principles of human brain organization (Friston, 2002). Specifically, although the function of an area at a given cortical location is highly specialized, the information it processes is dependent on its precise connections with other areas in different parts of the brain (Varela et al., 2001). Large-scale functional interactions between spatially distinct neuronal assemblies can be assessed using functional connectivity methods, which estimate statistical dependence between the dynamic activities of distinct brain areas (Friston, 2011). Functional connectivity is most often measured using functional magnetic resonance imaging (fMRI) data, which have a spatial resolution of a few millimeters and permit to construct accurate maps of large-scale functional networks across the brain (Fox and Raichle, 2007; Ganzetti and Mantini, 2013). However, a significant drawback in the context of functional connectivity is that fMRI provides only an indirect measure of brain activity mediated by a slow hemodynamic response. Alternatively, electroencephalography (EEG) or magnetoencephalography (MEG) can be utilized to estimate large-scale functional interactions within large-scale brain networks. Despite a number of technical limitations, they are potentially more suited to investigating mechanisms of long-range neuronal communication, insofar as they yield high temporal resolution and directly measure electrophysiological activity (Ganzetti and Mantini, 2013; Pfurtscheller and Lopes da Silva, 1999).

In recent years, technological advances have enabled the reliable reconstruction of ongoing activity in the brain (typically called 'source space') using MEG (Mantini et al., 2011). These developments have permitted to confirm the electrophysiological basis of fMRI-based connectivity (Brookes et al., 2011; Hipp et al., 2012). For instance, band-limited MEG power across distant brain regions was found to be temporally coherent during rest, and spatially organized similarly to resting state networks (RSNs) previously identified using fMRI (Brookes et al., 2011; de Pasquale et al., 2010). Moreover, MEG studies have begun to disclose important

information about brain network dynamics also during task performance (de Pasquale et al., 2012; Hipp et al., 2011), suggesting that long-range neuronal communication is characterized by rapid changes of synchronized oscillatory activity within specific brain circuits (de Pasquale et al., 2010). However, applications of MEG for large-scale studies remain limited, mainly because MEG is not portable and has high maintenance costs.

There may be several reasons why no research group has been able to map brain networks using EEG, as previously done using fMRI (Fox and Raichle, 2007; Ganzetti and Mantini, 2013; Gillebert and Mantini, 2013) and MEG (Brookes et al., 2011; de Pasquale et al., 2010; Hipp et al., 2012). One of the main technical difficulties to obtain RSNs from EEG signals is that the high requirement of accurate and precise source activity reconstructions. Unlike MEG, source analysis of EEG potentials requires indeed precise, realistic biophysical models that incorporate the exact positions of the sensors as well as the properties of head and brain anatomy, such that appropriate source localization techniques can be applied to map surface potentials to cortical sources (Michel et al., 2004). To build a realistic head model, accurate representation of the volume conductor of the head and precise volume conductivity of each tissue are essential (Cho et al., 2015; Fiederer et al., 2015; Haueisen et al., 1997; Ramon et al., 2006). Moreover, spatial sampling density and coverage of EEG electrodes also play a crucial role for neuronal source estimation (Slutzky et al., 2010; Song et al., 2015). High-density EEG (hdEEG) provides both high spatial sampling density and large head coverage, which facilitates the reconstruction of brain activity in the source space. Many research groups working with EEG still make use of low-density systems with 32 or 64 channels, whereas hdEEG systems are not widespread yet. Also, dedicated processing tools that permit to use hdEEG for brain imaging in a manner that is analogous to MEG are currently lacking. Another concern to study RSNs with EEG (also with MEG) is the so-called 'signal leakage' across brain voxels (Brookes et al., 2012; Hillebrand et al., 2012; Hipp et al., 2012). In EEG studies, the leakage problem can be caused by volume conduction as well as the ill-posed nature of the inverse solutions. While the former occurs inevitably during the signal recording and at a sensor level, the latter is due to

the fact that EEG/MEG source estimation consists of estimating a few thousand voxel activities from maximally a few hundred recordings. Therefore, the source estimation is underspecified in nature and yields a blurred image of the true activity in the brain voxels where activity estimated in one voxel is in fact a weighted sum of the activities in the neighboring voxels. Thus, we suggest that a combination of three approaches could be used to alleviate the leakage problem for the EEG source estimation in order to extract the long-range connectivity and networks: 1) increasing the degrees of freedom of the sensor recordings; 2) an appropriate choice of source estimation method and 3) using a connectivity method that minimizes the effects of signal leakage.

Here we propose that higher degrees of freedom needed to correctly resolve the dynamics of brain activity can be achieved through increasing the number of sensors by utilizing hdEEG. Furthermore, since there are no restrictions on the locations of active sources in resting state networks, we have used distributed source models that aim at minimizing the leakage among the brain voxels and have tested for different methods within two major families of minimum norm source estimators and beamformers. Finally, in order to obtain an estimate of connectivity that is least affected by the leakage problem, we have employed independent component analysis (ICA). Notably, MEG studies documented that the signal leakage problem is less critical when detecting RSNs with ICA than seed-based connectivity analysis (Brookes et al., 2011). ICA performs a blind decomposition of a given number of spatio-temporal patterns that are mixed in the data, assuming that these patterns are mutually and statistically independent in space (sICA) or time (tICA). For fMRI analyses, the use of sICA is warranted because the number of time points is typically much smaller than that of brain voxels, and this possibly leads to unreliable data decomposition by tICA (McKeown et al., 1998). However, tICA has been preferred in EEG/MEG connectivity studies (Brookes et al., 2011; Yuan et al., 2016). In the case of EEG/MEG, the use of tICA is possibly not problematic due to the higher temporal resolution of these techniques as compared to fMRI. No study has

ever tested whether and to what extent sICA can successfully retrieve brain networks from EEG/MEG data.

In this study, we describe a complete pipeline for the detection of EEG RSNs, which exploits the advantages of high-density as compared to low-density EEG systems and includes state-of-the-art tools for data preprocessing, realistic head model generation, source localization and ICA-based connectivity analysis. We show for the first time that EEG RSNs obtained using sICA are substantially more robust as compared to those produced by tICA. Most importantly, such EEG RSNs have minimal or no signal leakage as well as a spatial accuracy comparable to that of fMRI RSNs. Notably, hdEEG data can be collected simultaneously with fMRI and also in combination with non-invasive brain perturbation by transcranial magnetic stimulation (TMS) or transcranial direct/alternating current stimulation (tDCS/tACS). Furthermore, hdEEG experiments can be easily performed not only in healthy volunteers but also in neurological and psychiatric patients. Our methodological work may therefore open up new exciting research avenues in neuroscience, and contribute to rise of hdEEG as a powerful tool for both basic and translational investigations on human brain networks.

2. Materials and Methods

2.1 Description of the analysis workflow

We developed a complete analysis workflow to obtain multiple subject-specific RSNs from hdEEG recordings (Fig.1). Four main analysis steps are involved: 1) *Data preprocessing,* to attenuate noise and artifacts that are mixed in the data; 2) *Volume conduction model creation,* to establish how brain sources (i.e. ionic currents in the cortex) can generate specific distributions of potentials over the hdEEG sensors; 3) *Brain activity reconstruction,* to estimate -based on the EEG recordings and the head model- the distribution of active brain sources that most likely generates the potentials measured over the hdEEG sensors; 4) *Connectivity analysis*, to obtain RSN maps showing brain regions that have similar modulations of band-limited power, and are

therefore thought to preferentially interact with each other. The software implementing the analysis workflow described above is freely available, and can be found at http://www.bindgroup.eu/index.php/software.

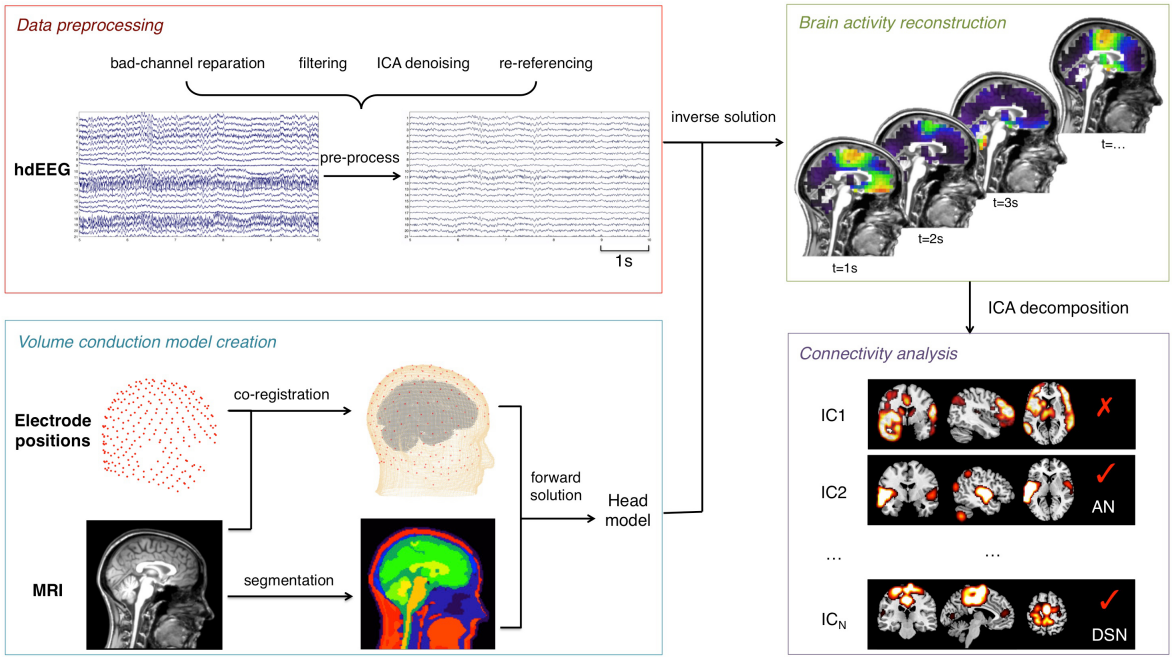

Fig.1 – Pipeline for obtaining single-subject RSNs from hdEEG recordings. The main analysis steps include: 1) Data preprocessing, involving bad-channel detection, filtering, ICA-denoising and re-referencing; 2) Volume conduction model creation, involving electrodes co-registration, MRI segmentation and forward modeling solution; 3) Brain activity reconstruction, to estimate the distribution of active brain sources that most likely generates the potentials measured over the hdEEG sensors; 4) Connectivity analysis, extracting independent components from the power time series of voxels and selecting the components associated with large-scale brain network activity.

2.1.1 Data preprocessing

First of all, we detected channels with low signal quality and labeled them as 'bad channels'. To this end, we used an automated procedure that combines information from two different parameters. The first parameter was the minimum Pearson correlation of the signal in a frequency band of interest (here we selected the band 1-80Hz) against all the signals from the other channels. The second parameter was the noise variance, estimated in band in which the contribution of the EEG signal can be considered negligible (here we selected the band 200-

250Hz). We define bad channels those for which at least one of the two channel-specific parameters were outliers as compared to the total distribution of values. To ensure robustness of the detection, the threshold to define an outlier was set at equal to $m+4s$, where m is the average value and s is the standard deviation. The detected bad channels were interpolated by using information from the neighboring channels, as implemented in the FieldTrip toolbox (http://www.fieldtriptoolbox.org). Later, we band-pass filtered the data in the frequency range 1-80Hz and we applied independent component analysis (ICA) in order to remove of ocular and muscular artifacts (Mantini et al., 2008). A fast fixed-point ICA (FastICA) algorithm (http://research.ics.aalto.fi/ica/fastica) using a deflation approach and hyperbolic tangent as contrast function was used to extract independent components (ICs). After ICA decomposition, the artifactual ICs were automatically classified by extracting and assessing the following parameters: 1) correlation c_p between the power of the IC with vertical electrooculogram (vEOG), horizontal electrooculogram (hEOG) and electromyogram (EMG) (see Supplementary Fig. 1); 2) the coefficient of determination r^2 obtained by fitting the IC power spectrum with a 1/f function; 3) the kurtosis k of the IC. An IC was classified as artifactual if at least one of the above parameters was above a given threshold (Supplementary Table 1), which was set in accordance with previous studies (de Pasquale et al., 2010; Mantini et al., 2009). Finally, following artifact rejection we re-referenced the EEG signals using the average reference approach, which showed to be both robust and accurate when using hdEEG data (Liu et al., 2015).

2.1.2 Volume conduction model creation

Precision and accuracy are essential to retrieve the electrical activity origins in the brain. Specifically, obtaining an accurate EEG forward solution requires the generation of realistic volume conductor model from an individual MR image and the definition of correct electrodes locations with respect to it.

Since electrode positions and MR anatomy are not in the same space, we spatially coregistered the EEG electrodes to MR space (Supplementary Fig.2). This procedure consisted of three distinct steps. In the first step, we estimated the positions of three anatomical landmarks (nasion, left and right preauricolar) in the MR image by projecting the corresponding predefined MNI coordinates ([0, 85, -30], [-86, -16, -40] and [86, -16, -40]) to individual space. Then, we calculated a rigid-body transformation to match the three landmarks in electrode space to the corresponding landmarks in MR space, and applied it to the electrode positions (Supplementary Fig. 2A). In the second step, we aligned the electrode positions to the surface of the head extracted from individual MR image (Supplementary Fig. 2B) using the Iterative Closest Point (ICP) registration algorithm (Besl and Mckay, 1992). In the third and last step, we ensured that each electrode was perfectly lying over the head surface by projecting it onto the surface point with the smallest Euclidean distance (Supplementary Fig. 2C).

A realistic head model requires the definition of multiple tissue classes of the head, each characterized by a specific conductivity value. We opted for a solution involving 12 tissue classes (skin, eyes, muscle, fat, spongy bone, compact bone, cortical gray matter, cerebellar gray matter, cortical white matter, cerebellar white matter, cerebrospinal fluid and brain stem), which represents the current state-of-the-art for studies modeling the effect of electrical stimulation on the brain (Holdefer et al., 2006; Wagner et al., 2014). This is putatively more accurate than other solutions typically used in EEG analysis, and involving five or less tissue classes (Fuchs et al., 2002; Wolters et al., 2006). Given the intrinsic difficulty in defining all 12-tissue classes directly from the MR image (Supplementary Fig. 3), we warped a high-resolution head template to subject space using the normalization tool in SPM12 (http://www.fil.ion.ucl.ac.uk/spm/software/spm12). This head template was obtained from the ITIS foundation of ETH Zurich (http://www.itis.ethz.ch/virtual-population/regional-human-models/mida-model/mida-v1-0) (Iacono et al., 2015). The conductivity value associated with each tissue class was defined based on relevant literature (Haueisen et al.,

1997), and is in line with recent brain stimulation studies (Holdefer et al., 2006) (Supplementary Table 2).

For the numerical approximation of the volume conduction model, we used the whole-head finite element method (FEM) technique. FEM have been proven to be very effective for solving partial differential equations with complicated solution domain and boundary conditions (Wolters et al., 2004). A prerequisite for FEM is the generation of a mesh that represents the geometric and electric properties of the head volume conductor. A hexahedral mesh (i.e. the points of the mesh are connected to create hexahedrons) of the 12 compartments was generated directly from the warped template image. The dipoles corresponding to brain sources were placed on a regular 6-mm grid spanning the cortical grey matter and cerebellar grey matter. In this study, the leadfield matrix L, which contains the measured potentials corresponding to each configuration of dipole position and orientation, was calculated using the Simbio FEM method integrated in FieldTrip. Based on the reciprocity principle, the scalp electric potentials can be expressed in the following equation with leadfield matrix.

$$\Phi = L \cdot J \qquad \text{(Eq.1)}$$

where $L \in \mathbb{R}^{N_E \times (3N_V)}$ is the leadfield matrix; $\Phi \in \mathbb{R}^{N_E \times 1}$ is the scalp electric potential; $J \in \mathbb{R}^{(3N_V) \times 1}$ is the current density at the source; N_E is the number of electrodes, and N_V the number of dipole sources in the cortical grey matter and cerebellar grey matter.

2.1.3 Brain activity reconstruction

We performed reconstruction of brain activity in the source space based on the hdEEG artifact-free recordings and the volume conduction model. To this end, we used the exact low-resolution brain electromagnetic tomography (eLORETA) to perform source reconstruction (Pascual-Marqui et al., 2011). The primary feature of the eLORETA algorithm is that of yielding zero localization error to point sources under ideal (noise-free) conditions. eLORETA estimates the matrix of source activity in the brain J based on the following formula:

$$J = W^{-1} \cdot L \cdot (L \cdot W^{-1} \cdot L^T + \alpha H)^+ \cdot \Phi \quad \text{(Eq.2)}$$

where the superscript + denotes the Moore-Penrose pseudoinverse, α >0 is the Tikhonov regularization parameter, $W \in \mathbb{R}^{N_V \times N_V}$ is a symmetric positive definite weight matrix and $H \in \mathbb{R}^{N_E \times N_E}$ is a matrix that depends on the EEG reference. Since the EEG data are in average reference, $H = I - \frac{1}{N_E} 1$, where $I \in \mathbb{R}^{N_E \times N_E}$ is the identity matrix; $1 \in \mathbb{R}^{N_E \times N_E}$ where all elements are equal to 1.

The regularization parameter α was estimated by covariance matrix of the noise in measurements, $\sum_{\Phi}^{noise}$, with $\sum_{\Phi}^{noise} = \alpha H$. The weight matrix W was iterated until the convergence with $w_i = \sqrt{L_i^T \cdot (L \cdot W^{-1} \cdot L^T + \alpha H)^+ \cdot L_i}$, where w_i (i=1, 2, ..., N_V) is the element of the diagonal weight matrix W.

By estimating the matrix J (see Eq. 2), we obtained the oscillation strength in each dipole with x, y and z orientations at each temporal moment, indicated with $j_x(t)$, $j_y(t)$ and $j_z(t)$ respectively, we obtained the power time series p(t) by means of the following formula:

$$p(t) = \sqrt{j_x^2(t) + j_y^2(t) + j_z^2(t)} \quad \text{(Eq.3)}$$

One important issue to measure large-scale connectivity is the effects of signal transmission delays between the distant brain regions (Deco et al., 2011). To avoid the impacts of time delay between long-range sources, we downsampled the power time series to 1 Hz, following an established approach that was proposed in MEG connectivity studies (Brookes et al., 2011). This downsampling can enhance the temporal correlations between brain regions which permits a more accurate detection of slow fluctuation of band-limited power (Supplementary Fig. 4), and is also well matched with the infra slow fluctuations of the blood oxygen level dependent (BOLD) signal (Palva and Palva, 2012).

2.1.4 Connectivity analysis

Connectivity analysis based on the reconstructed power timecourses across voxels was performed using ICA, in either its spatial or temporal version (Supplementary Fig.5). ICA yields a number of independent components (ICs), each of which consists of a spatial map and an associated time-course. The IC spatial map reveals brain regions that have a similar response pattern, and are therefore functional connected (Brookes et al., 2011; Mantini et al., 2007b). The number of ICs was estimated by using the minimum description length (MDL) criterion (Li et al., 2007). The FastICA algorithm was run 10 times using a deflation approach and hyperbolic tangent as contrast function to extract reliable ICs, as estimated by the ICASSO software package (Himberg and Hyvarinen, 2003) (http://research.ics.aalto.fi/ica/icasso). EEG-RSNs of interest were selected by using a template-matching procedure. First, the templates were warped to individual MR space, in which the EEG-RSNs were defined. The Pearson correlation was used to estimate the similarity in the spatial distribution of the EEG-ICs and the template RSN maps (Supplementary Fig.6). The best EEG-IC match for each template map was extracted iteratively, labeled as a specific EEG-RSN, and removed from the pool of EEG-ICs. This impedes that the same IC were erroneously associated to two different templates.

2.2 Application to real hdEEG data and testing

2.2.1 Data acquisition

Data used in this study comprise resting-state hdEEG signals, electrode positions and individual whole-head anatomy MRI from nineteen healthy right-handed subjects (age 28 $\pm$ 5.9 years, 5 males and 14 females). All participants reported normal or corrected-to-normal vision, had no psychiatric or neurological history, were free of psychotropic or vasoactive medication. Before undergoing the examination, they gave their written informed consent to the

experimental procedures, which were approved by the local Institutional Ethics Committee of ETH Zurich.

The EEG experiment was performed in accordance with the approved guidelines, in a quiet, air-conditioned laboratory with soft natural light. Continuous 5-minute resting EEG data with eyes open were collected. To reduce eye movements and blinks, subjects were instructed to keep fixation on the center of screen during the experiment. High-density EEG signals were recorded at 1000 Hz by the 256-channel HydroCel Geodesic Sensor Net (GSN) using silver chloride–plated carbon-fiber electrode pellets provided by Electrical Geodesics (EGI, Eugene, Oregon, USA). During recording, the EGI system used the electrode at vertex (labeled as Cz in the 10/20 international system) as physical reference. In addition, to better characterize the scalp distribution of EEG signals, all 256 sensors and three landmarks positions (nasion, left and right preauricolar) were localized prior to the EEG acquisition by using a Geodesic Photogrammetry System (GPS). In detail, GPS derives the position of each EEG electrode from multiple pictures, simultaneously captured, of all the sensors on the subject's scalp. After defining the 2D electrode positions on at least 2 pictures, 3D coordinates are computed by using a triangulation algorithm (Russell et al., 2005). In addition to EEG data and electrode position information, a T1-weighted whole-head MR image of each subject was acquired in a separate experimental session using a Philips 3T Ingenia scanner with a turbo field echo sequence. The scanning parameters were: TR=8.25ms, TE=3.8ms, 8° flip angle, 240×240×160 field of view, 1 mm isotropic resolution.

2.2.2 Analyses on the obtained RSNs

First, we applied our hdEEG processing pipeline and reconstructed power envelopes of oscillatory cortical activity from each hdEEG dataset. For sICA analysis, based on the results of the MDL analysis (Li et al., 2007), we run sICA requiring 34 to 58 ICs, depending on the specific hdEEG dataset. We attempted the detection of EEG-RSNs also with tICA, following the network detection approach suggested in previous EEG/MEG connectivity studies (Brookes et al., 2011).

In the case of both sICA and tICA, we used as templates for RSN detection the maps obtained using from fMRI data used in one of our previous studies (Mantini et al., 2013). These data, which were collected in 24 healthy young subjects at rest for 20 minutes, were split in two equal parts of 10 minutes. Brain networks were detected using sICA from each dataset. As for the methods used, please refer to our previous work (Mantini et al., 2013). The first dataset was used to generate fMRI template maps to be used for comparison with EEG networks, whereas the second dataset was employed for a test-retest fMRI-RSN analysis. The RSN template maps obtained from fMRI data corresponded to: default mode network (DMN), dorsal attention network (DAN), ventral attention network (VAN), right frontoparietal network (rFPN), left frontoparietal network (lFPN), language network (LN), cingulo-opercular network (CON), auditory network (AN), ventral somatomotor network (VSN), dorsal somatomotor network (DSN), visual foveal network (VFN), visual peripheral network (VPN), medial prefrontal network (MPN) and lateral prefrontal network (LPN) (see Supplementary Fig. 2). For each EEG-RSN, we transformed the individual maps to common space using SPM and derived a group-level RSN map by using performing a voxel-wise non-parametric permutation test by FSL (http://fsl.fmrib.ox.ac.uk/fsl/fslwiki). We used 5000 permutations for this across-subject analysis, and we set the significance threshold to $p<0.01$ corrected for multiple comparisons by using the threshold-free cluster enhancement (TFCE) method (Smith and Nichols, 2009). To verify that the detected EEG-RSNs were selectively associated with a specific fMRI-RSN, we calculated a matrix of cross-correlations between EEG-RSN and fMRI-RSN maps. Also we checked the spatial correlation of the matching ICs and mismatching ICs. Moreover, we tested the robustness RSN spatial patterns obtained by sICA/tICA, by performing a split-half analysis. Specifically, we split the 5-minute recording into two segments of equal duration. We independently obtained EEG-RSNs from each of these two data segments using our analysis pipeline. Finally, we examined the correspondence between the two sets of maps by using the Pearson correlation between RSN maps. For both tICA and sICA, we also examined the correlations between maps for matching ICs and mismatching ICs, respectively.

As a further analysis step, we investigated the impact of the number of EEG channels, the accuracy of the head model and the kind of source localization for an accurate RSN detection. Also in this case, performance was measured in terms of spatial correlation between EEG-RSNs to the fMRI-RSNs. To investigate the RSNs with lower montage density, we spatially subsampled each set of 256-channel recordings and derived 32-channel, 64-channel and 128-channel recordings with electrodes positioned according to standard EEG montages. The effect of using a less accurate head model was tested by running RSN detection on source data reconstructed using a 5-layer realistic FEM, and a 3-layer boundary element method (BEM) based either on an individual or a template MR image. In line with previous literature (Cho et al., 2015; Ramon et al., 2006; Wolters et al., 2006), the 5-layer FEM model comprised grey matter (cortical and cerebellar), white matter (cortical and cerebellar) plus brainstem, cerebrospinal fluid, skull (compact and spongy) and all remaining soft tissues (skin, eyes, muscles and fat). In turn, the 3-layer BEM models included brain plus cerebellum, skull and all other tissues. We obtained the conductivity values for 5- and 3-layer models by pooling together different tissues and averaging the conductivity values used for the 12-layer head model. Finally, we examined whether it is possible to detect EEG-RSNs using different source localization methods for the reconstruction of brain activity in the source space. To this end, we tested the RSN results obtained using eLORETA against those provided by sLORETA (Pascual-Marqui, 2002) and MNE (Wang et al., 1992), two other minimum norm methods, and LCMV (VanVeen et al., 1997), a beamforming method.

3. Results

We applied this processing pipeline to 256-channel hdEEG data collected in 19 young healthy participants, who were instructed to fixate a centrally presented cross for 5 minutes. After reconstructing power envelopes of oscillatory cortical activity for each voxel in the grey matter, we applied ICA for the detection of multiple RSNs from each hdEEG dataset.

Connectivity analyses were conducted in individual space by applying either temporal ICA (tICA) or spatial ICA (sICA) (Supplementary Fig. 1) on power envelopes of oscillatory activity, and the resulting maps were transformed to common space to enable across-subject statistical analyses.

First, we attempted to obtain brain networks by applying tICA to the source-space power envelopes (Fig. 2A). We defined 14 EEG-RSNs in each of the 19 subjects: default mode network (DMN), dorsal attention network (DAN), ventral attention network (VAN), right frontoparietal network (rFPN), left frontoparietal network (lFPN), language network (LN), cingulo-opercular network (CON), auditory network (AN), ventral somatomotor network (VSN), dorsal somatomotor network (DSN), visual foveal network (VFN), visual peripheral network (VPN), medial prefrontal network (MPN) and lateral prefrontal network (LPN). After retrieving the 14 RSNs using tICA, we also performed network detection using sICA and we compared the resulting maps (Fig. 2B).

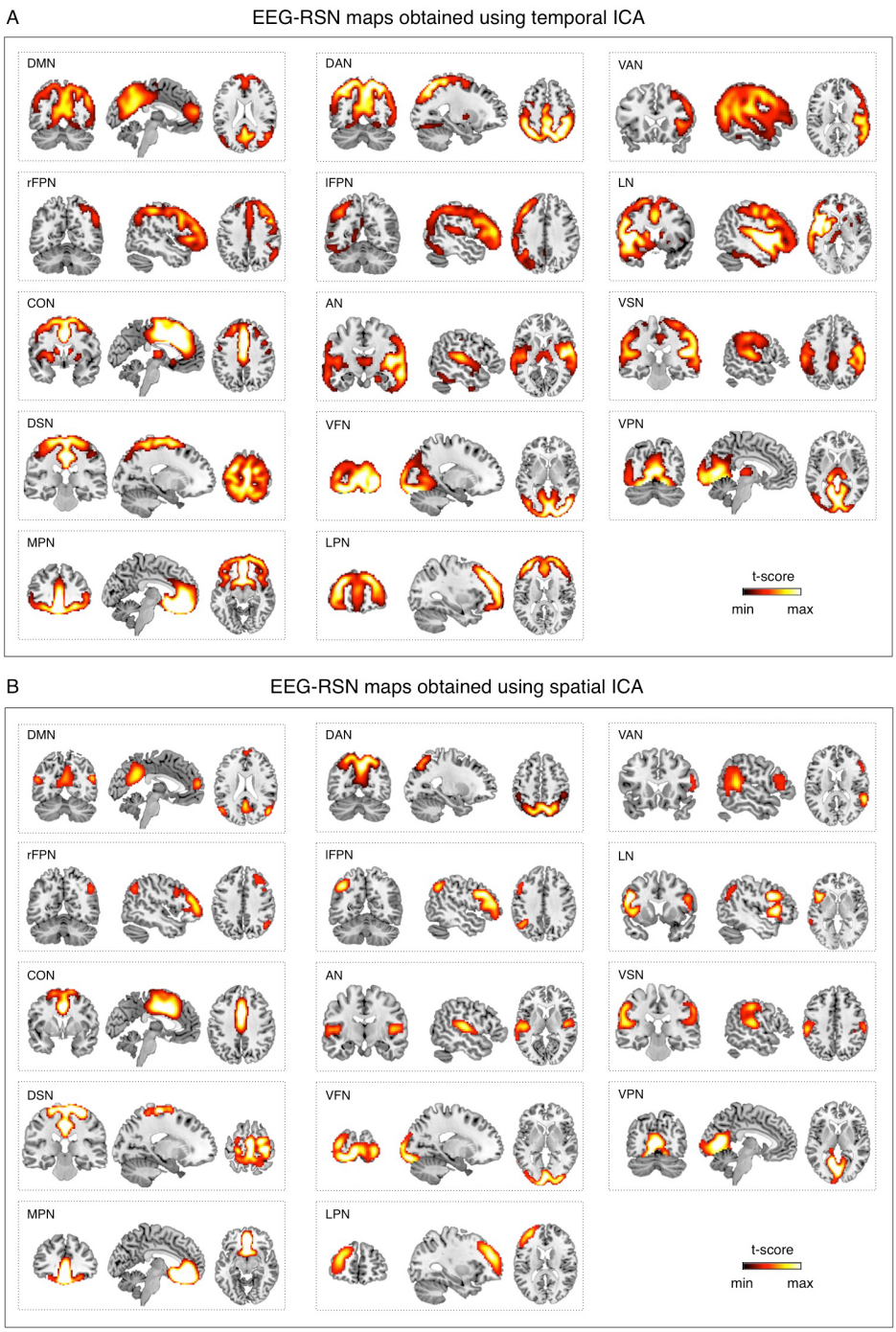

Fig.2 – Group-level maps for large-scale brain networks extracted from hdEEG data. EEG networks were obtained using (A) tICA or (B) sICA, and were selected and labeled on the basis of the spatial overlap with fMRI networks: default mode network (DMN), dorsal attention network (DAN), ventral attention network (VAN), right frontoparietal network (rFPN), left frontoparietal network (lFPN), language network (LN), cingulo-opercular network (CON), auditory network (AN), ventral somatomotor network (VSN), dorsal somatomotor network (DSN), visual foveal network (VFN), visual peripheral network (VPN), medial prefrontal network (MPN) and lateral prefrontal network (LPN). The hdEEG networks were first identified in each subject, and then subjected to non-parametric group-level testing (threshold: $p<0.01$, TFCE corrected). Spatial maps are shown in coronal, sagittal and axial sections.

We observed that the EEG-RSN maps obtained with sICA, as compared to those obtained by tICA, had larger spatial correlations with corresponding fMRI-RSNs (paired t-test, p=0.0129) (Fig. 3A-C). Notably, the difference between correlation values obtained for matching and non-matching RSNs was significantly higher for sICA (unpaired t-test, p=0.0218). Overall, the correlation values between group-level EEG- and fMRI-RSNs extracted using sICA (r=0.53±0.08) were in a range comparable with those obtained between the fMRI-RSNs used as template and the networks obtained by sICA using a replication fMRI dataset (r= 0.60±0.12). To further test the robustness of our results in individual subjects, we conducted a split-half analysis. We found that ICA on hdEEG signals was able to reconstruct EEG-RSNs even on data segments of only 2.5 minutes (Supplementary Fig. 7 and Supplementary Fig. 8), with high values of spatial correlation between network maps from the two segments (Fig. 3D-F).

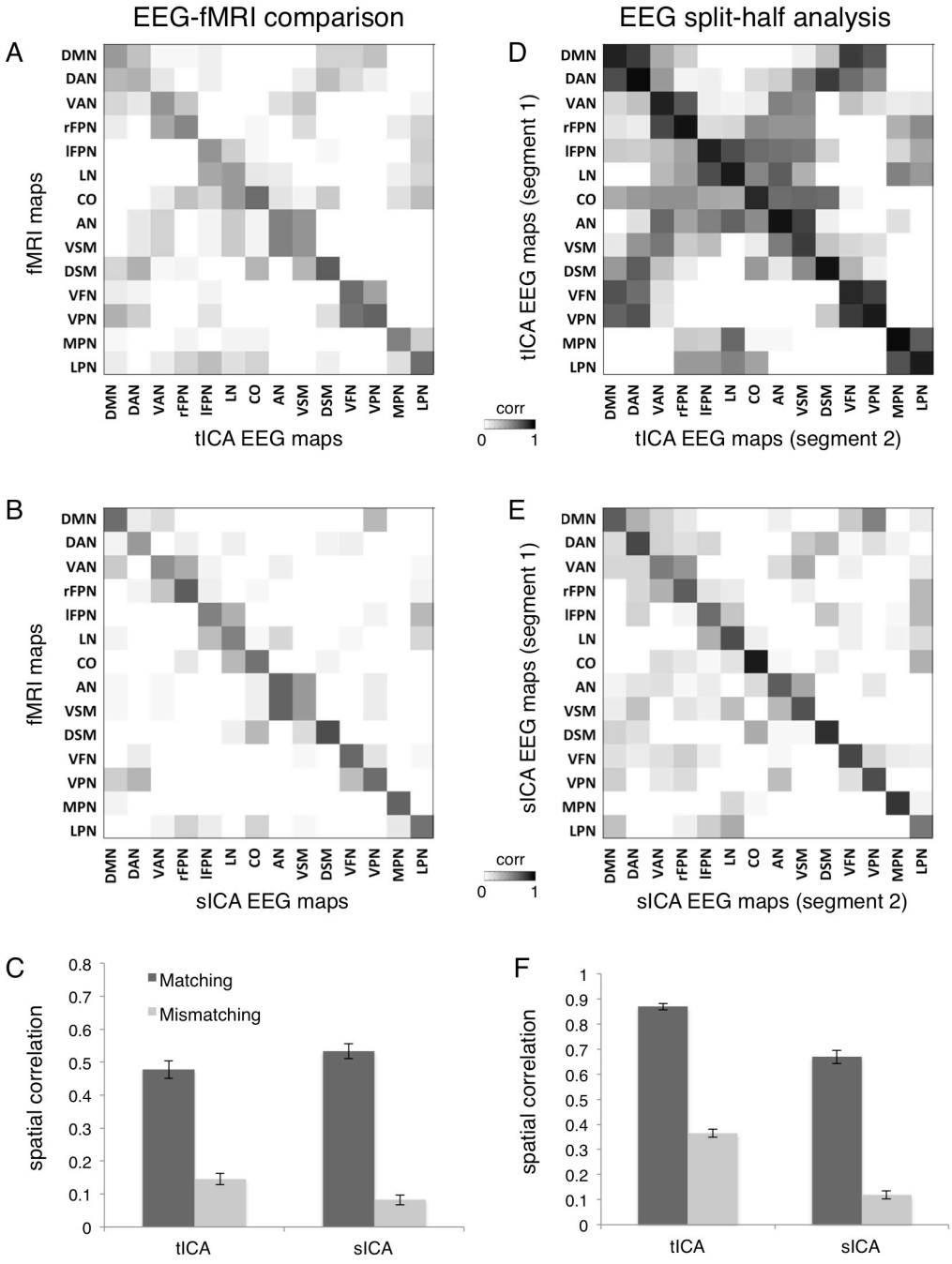

Fig.3 – Analysis of robustness for ICA-based RSNs. (A) cross-correlation between spatial maps from tICA and fMRI templates; (B) cross-correlation between spatial maps from sICA and fMRI templates; (C) bar plot of correlations between matching and mismatching RSNs, obtained using either tICA or sICA. (D) cross-correlation between RSNs obtained using tICA from two equally long EEG segments; (E) cross-correlation between RSNs obtained using sICA from two equally long EEG segments; (F) bar plot of correlations between matching and mismatching RSNs, obtained using either tICA or sICA from two equally long EEG segments.

Our results provided evidence for a robust EEG RSN extraction using sICA. To better understand to what extent the sICA results depended on the use of hdEEG, we performed more detailed analyses. First, we examined the influence of the montage density by comparing the RSNs obtained using 32-, 64, 128- and 256-channel EEG. The latter yielded the highest values of spatial correlation with the template maps, but the difference with 128-channel EEG was not significant (Fig. 4A). Also, our analyses confirmed that network reconstruction was more accurate with a head model based on 12-layer FEM as compared to 5-layer FEM and 3-layer boundary element method (BEM) model built on an individual MR image, as well as a 3-layer BEM built using a template MR image. Yet, the use of a less precise head model had smaller impact on the RSN reconstruction than a reduced montage density (Fig. 4B). Also, we found eLORETA source localization to be only slightly superior to exact low-resolution brain electromagnetic tomography (sLORETA), whereas the reconstruction improvement as compared to minimum norm estimate (MNE) and linearly constrained minimum variance (LCMV) methods were remarkable (Fig. 4C). The quantitative analyses assessing the impact of the EEG montage density, type of head model and use of source localization method were supported by visual inspection of the EEG-RSN maps (Fig. 5).

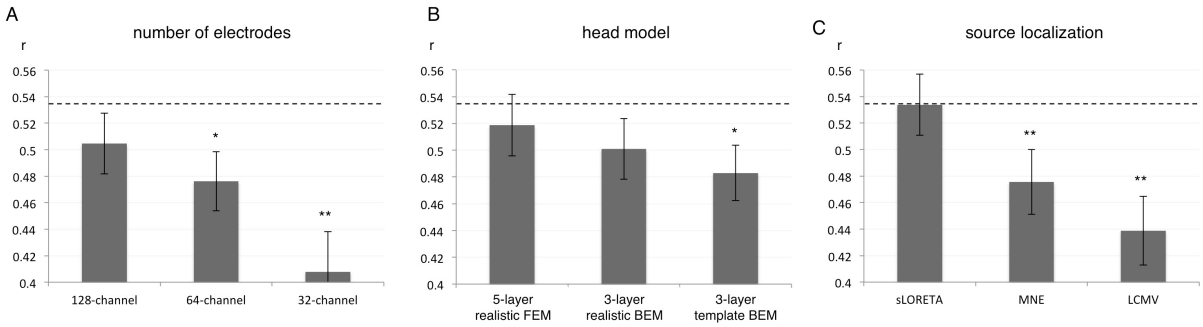

Fig.4 – Accuracy of RSN reconstruction with different EEG montage density, head model and source localization methods. Bar plots showing mean and standard error of the spatial correlations between corresponding fMRI-RSNs and EEG-RSNs (A) obtained by 128-, 64- and 32-channel recordings, using 12-layer realistic FEM and eLORETA source localization; (B) obtained by 5-layer realistic FEM, 3-layer realistic BEM and 3-layer template BEM, using 256-channel recordings and eLORETA source localization; (C) obtained by sLORETA, MNE and LCMV, using 256-channel recordings and 12-layer realistic FEM. The horizontal dashed line indicates the average correlation of corresponding fMRI-RSNs and EEG-RSNs obtained using 256-channel recordings, 12-layer realistic FEM and eLORETA source

localization (default configuration in the pipeline). The markers above the bars indicate statistically significant reduction between correlation values obtained using a specific configuration and the default configuration in the pipeline (one-tailed paired t-test: * = p<0.05; ** = p<0.01).

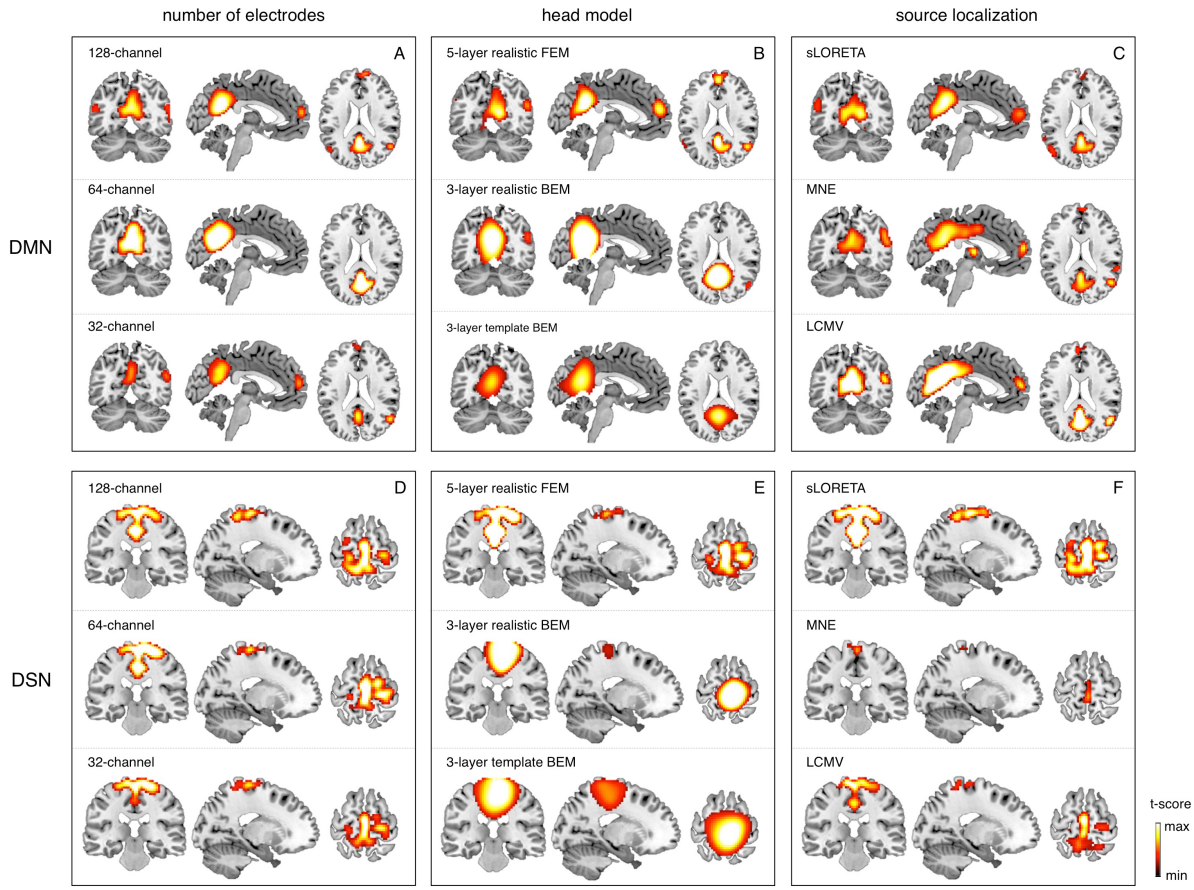

Fig.5 – Influence of EEG montage density, head model and source localization methods on network reconstruction. (A) DMN and (D) DSN maps obtained using 128-, 64- and 32-channel recordings respectively, using 12-layer realistic FEM and eLORETA source localization; (B) DMN and (E) DSN maps obtained using 5-layer realistic FEM, 3-layer realistic BEM and 3-layer template BEM respectively, using 256-channel recordings and eLORETA source localization; (C) DMN and (F) DSN maps obtained by sLORETA, MNE and LCMV localization respectively, using 256-channel recordings and 12-layer realistic FEM.

4. Discussion

The main goal of this study was the detection of large-scale brain networks from hdEEG data, with a spatial accuracy comparable to the one that can be obtained using fMRI. This is a particularly complex task, as it requires the precise estimation of neuronal activity in the cortex from recordings made over the scalp. To achieve that goal, we devised a processing pipeline that is tailored to hdEEG data and includes state-of-the-art analysis techniques such as appropriate data pre-processing, realistic head model construction, accurate source localization and ICA-based connectivity analysis. Our results demonstrated that the use of high-density EEG montage is crucial for RSN detection, and that also the accuracy of the head model and the kind of source localization used are important for accurate network reconstructions. To the best of our knowledge, only one EEG study attempted to reconstruct brain networks using tICA (Yuan et al., 2016), but failed to show maps that correspond to fMRI networks. Notably, we showed for the first time that sICA can be effectively used for the detection of EEG-RSNs that are largely matching previously reported fMRI-RSN maps.

4.1 High-density EEG for source-space analyses

In this study, we investigated the RSNs spatial patterns using hdEEG. Specifically, we integrated information from hdEEG data, realistic electrode positions and structural MR images. A number of previous studies examined functional connectivity with EEG signals (Smit et al., 2008); however, connectivity analyses were kept at the sensor level due to the low-density electrode coverage. Interpretation of the results of these studies is not straightforward, since EEG recordings contain a mix of neuronal activity from different brain regions. More recently, interest of the scientific community is shifting from low-density EEG toward high-density EEG, from sensor space analyses toward source space analyses, thanks to the technological development and the advanced computing capacity of computers. Our work contributed to the development of analysis tools specifically tailored to hdEEG, providing a novel way to investigate brain activity in a non-invasive manner, and with relatively accurate spatial and

temporal resolution. Our work emphasized the importance of high-density montages for the EEG-RSN studies (Fig. 4A), especially for the RSNs including distant brain regions such as the DMN (Fig. 2B and 5A); however RSNs with a less distributed pattern, as for instance DSN, were successfully reconstructed also with a low density EEG montage (Fig 5D). Moreover, previous work clearly showed the importance of accurate information on electrode positions is crucial for accurate EEG re-referencing (Liu et al., 2015) and source localization (Van Hoey et al., 2000; Wang and Gotman, 2001). However, this is still neglected in a considerable part of current EEG studies.

4.2 Forward model and solution to the inverse problem

Previous studies suggested that the use of a realistic head model is essential for retrieving EEG sources (Ramon et al., 2006) and for conducting connectivity analyses in the source space (Cho et al., 2015). In particular, the head model is used to find the scalp potentials that would result from hypothetical dipoles, or more generally from a current distribution inside the head. Accordingly, we paid particular attention to the construction of a realistic head model. First, we used a structural MR image for each subject rather than a template, which was used to achieve a detailed segmentation of the head tissues. A large number of previous studies modeled the head with three compartments, i.e. skull, skin and brain (Fuchs et al., 2002), or five compartments, i.e. skull, skin, white matter, gray matter and cerebrospinal fluid (Van Uitert et al., 2003). Arguing against this oversimplification, we used a finite element model (FEM) based on 12 different tissues, following the approach suggested by recent studies that modeled the effect of transcranial electrical stimulation of the brain (Holdefer et al., 2006; Wagner et al., 2014). Our performance analysis confirmed the importance of using a realistic head model built on the MR image of the subject's head (Figs. 4B and 5B,E). On the other hand, we observed only subtle improvements with a head model created with a 12-layer FEM as compared to 5-layer FEM. The improvement was more marked compared to 3-layer BEM, in which white matter and gray matter belong to the same layer and are assigned the same conductivity value.

In our pipeline, a realistic head model was used in our processing pipeline in combination with eLORETA for the reconstruction of ongoing brain activity in the source space. It is worth noting that the performance of source localization algorithms depends on source depth, on the noise level, on the number of recording electrodes and on the head model (Michel et al., 2004) and there is no general consensus about which source localization method delivers best performance for EEG (Michel et al., 2004). Our results confirmed the suitability of eLORETA, as well as sLORETA, for EEG connectivity investigations (Figs.4C and 5C,F), compared with MNE and LCMV. As a linear, weighted minimum norm inverse solution proposed as an improvement of the well-know LORETA, eLORETA has been found to be particularly accurate in the presence of low-noise signals (Pascual-Marqui et al., 2011) and suitable for the study of brain connectivity using EEG (Aoki et al., 2015). Above all, our quantitative analyses on the correspondence between EEG-RSNs and fMRI-RSNs (Figs. 3 and 4) lend support to our choices in terms of head modeling and source localization methods.

4.3 Network detection by ICA

We detected RSNs using independent component analysis (ICA) rather than alternative methods based on seed-based connectivity (Brookes et al., 2012; de Pasquale et al., 2010; de Pasquale et al., 2012), as ICA is a data-driven technique that can produce multiple RSNs by only imposing the constraint of either spatial or temporal independence between RSNs (sICA and tICA, respectively). sICA has been largely employed for the detection of RSNs with fMRI data, in which the number of time points is always much smaller than the number of voxels. In the case of EEG/MEG connectivity studies, tICA has been preferred to sICA since it is possibly better suited to capture the non-linear and non-stationary nature of neurophysiological signals (Brookes et al., 2011; Yuan et al., 2016). In this study, we showed for the first time that sICA can be successfully applied for the detection of RSNs from hdEEG data, and that the spatial patterns match better with previously published fMRI-RSNs (Fig. 2B and Supplementary Fig. 6).

Importantly, sICA seemed to provide more robust RSN detection than tICA, and to be minimally affected by the problem of signal leakage (Brookes et al., 2012) (Figs. 2 and 3). Our study has also the particular merit of showing RSNs that were previously reported only using fMRI but not MEG/EEG, such as VAN, AN and MPN (Mantini et al., 2013) (Fig. 2). A possible explanation for an increased sensitivity in RSN detection may be the fact that we extracted EEG-RSN maps at the single-subject level and in individual space, rather than transforming the source-space power time-courses to common space and performing a single ICA on concatenated time-courses from all subjects. The primary reason for our choice is methodological, and relies on the possibility to better incorporate information on head modeling and electrode positioning (Marino, 2016) in source activity reconstructions. However, it should also be considered that the extraction of RSNs at the single subject level may be important for clinical applications, and in particular for the study of stroke, multiple sclerosis, Alzheimer's disease and all other conditions in which brain plasticity (Johnston, 2004) may occur.

4.4 Study limitations and caveats

The pipeline for the analysis of hdEEG data includes several analysis steps. The successful detection – for the first time- of EEG-RSNs indirectly confirms that each of these steps yielded satisfactory results. From the methodological point of view, an important advancement was the creation of a realistic head model with 12 distinct compartments, which permits to better account for potential spatial distortions in the flow of currents from sources to sensors. It should be noted, however, that our head model did not consider tissue anisotropy. Considering anisotropy may lead to even more accurate results, in particular for subcortical regions (Cho et al., 2015; Wolters et al., 2006). Also, we used conductivity values derived from the literature. A potential improvement may come from the in-vivo estimation of head tissue conductivity, for which techniques are being developed (Akalin Acar et al., 2016; Lew et al., 2009) and may be available in the next future. Another potential limitation of the present study pertains to the use of ICA for network detection. Specifically, the number of ICs

extracted from the EEG power timecourses was performed using the MDL approach, in line with previous fMRI-RSN studies (Li et al., 2007). Of note, we did not examine how the use of different IC numbers impacts on the quality of the detected RSNs. Future studies are warranted to evaluate if EEG-RSN detection can be further improved by using alternative approaches to estimate the number of ICs.

5. Conclusion

In this study, we successfully detected large-scale brain networks using hdEEG data, based on a robust methodology for noise and artifact reduction, head modeling and source localization. The development of such methodology may have broader impact on the field of brain imaging and neuroscience. We posit that hdEEG can constitute a powerful tool for investigating temporal and spectral signatures of long-range functional connectivity in health and disease. Notably, the characterization of functional connectivity dynamics using fMRI is problematic, given the relatively low temporal resolution of the technique. In contrast, EEG – as well as MEG- permits examining network reconfiguration at very fast time scale. Moreover, the combination of hdEEG with simultaneous fMRI can unravel the direct relationship between functional connectivity measured through electrophysiological and hemodynamic techniques (Mantini et al., 2007b). Finally, analyses of functional connectivity based on hdEEG data may be particularly relevant in a clinical context. In particular, the use of functional connectivity measures from hdEEG has the potential to provide novel and more sensitive biomarkers to improve diagnostics.

Acknowledgements

The authors would like to thank Joshua Balsters and Marc Bächinger for providing structural MR images based on which head models were built and also Zhiliang Long for scientific discussion about the similarities between EEG and fMRI networks. The work was supported by

the Chinese Scholarship Council (scholarship 201306180008 to QL), the Swiss National Science Foundation (grants 320030_146531 and P1EZP3_165207), the Seventh Framework Programme European Commission (grant PCIG12-334039), the KU Leuven Special Research Fund (grant C16/15/070), and the Research Foundation Flanders (FWO) (grants G0F76.16N and G0936.16N).

Competing financial interests

The authors declare no competing financial interests.

References

Akalin Acar, Z., Acar, C.E., Makeig, S., 2016. Simultaneous head tissue conductivity and EEG source location estimation. Neuroimage 124, 168-180.

Aoki, Y., Ishii, R., Pascual-Marqui, R.D., Canuet, L., Ikeda, S., Hata, M., Imajo, K., Matsuzaki, H., Musha, T., Asada, T., Iwase, M., Takeda, M., 2015. Detection of EEG-resting state independent networks by eLORETA-ICA method. Frontiers in Human Neuroscience 9, 31.

Besl, P.J., Mckay, N.D., 1992. A Method for Registration of 3-D Shapes. Ieee Transactions on Pattern Analysis and Machine Intelligence 14, 239-256.

Brookes, M.J., Woolrich, M., Luckhoo, H., Price, D., Hale, J.R., Stephenson, M.C., Barnes, G.R., Smith, S.M., Morris, P.G., 2011. Investigating the electrophysiological basis of resting state networks using magnetoencephalography. Proc Natl Acad Sci U S A 108, 16783-16788.

Brookes, M.J., Woolrich, M.W., Barnes, G.R., 2012. Measuring functional connectivity in MEG: a multivariate approach insensitive to linear source leakage. Neuroimage 63, 910-920.

Cho, J.H., Vorwerk, J., Wolters, C.H., Knosche, T.R., 2015. Influence of the head model on EEG and MEG source connectivity analyses. Neuroimage 110, 60-77.

de Pasquale, F., Della Penna, S., Snyder, A.Z., Lewis, C., Mantini, D., Marzetti, L., Belardinelli, P., Ciancetta, L., Pizzella, V., Romani, G.L., Corbetta, M., 2010. Temporal dynamics of spontaneous MEG activity in brain networks. Proc Natl Acad Sci U S A 107, 6040-6045.

de Pasquale, F., Della Penna, S., Snyder, A.Z., Marzetti, L., Pizzella, V., Romani, G.L., Corbetta, M., 2012. A cortical core for dynamic integration of functional networks in the resting human brain. Neuron 74, 753-764.

Deco, G., Jirsa, V.K., McIntosh, A.R., 2011. Emerging concepts for the dynamical organization of resting-state activity in the brain. Nature Reviews Neuroscience 12, 43-56.

Fiederer, L.D., Vorwerk, J., Lucka, F., Dannhauer, M., Yang, S., Dumpelmann, M., Schulze-Bonhage, A., Aertsen, A., Speck, O., Wolters, C.H., Ball, T., 2015. The role of blood vessels in high-resolution volume conductor head modeling of EEG. Neuroimage 128, 193-208.

Fox, M.D., Raichle, M.E., 2007. Spontaneous fluctuations in brain activity observed with functional magnetic resonance imaging. Nat.Rev.Neurosci. 8, 700-711.

Friston, K., 2002. Beyond phrenology: what can neuroimaging tell us about distributed circuitry? Annu Rev Neurosci 25, 221-250.

Friston, K.J., 2011. Functional and effective connectivity: a review. Brain Connect. 1, 13-36.

Fuchs, M., Kastner, J., Wagner, M., Hawes, S., Ebersole, J.S., 2002. A standardized boundary element method volume conductor model. Clin Neurophysiol 113, 702-712.

Ganzetti, M., Mantini, D., 2013. Functional connectivity and oscillatory neuronal activity in the resting human brain. Neuroscience 240, 297-309.

Gillebert, C.R., Mantini, D., 2013. Functional connectivity in the normal and injured brain. Neuroscientist. 19, 509-522.

Haueisen, J., Ramon, C., Eiselt, M., Brauer, H., Nowak, H., 1997. Influence of tissue resistivities on neuromagnetic fields and electric potentials studied with a finite element model of the head. IEEE Trans Biomed Eng 44, 727-735.

Hillebrand, A., Barnes, G.R., Bosboom, J.L., Berendse, H.W., Stam, C.J., 2012. Frequency-dependent functional connectivity within resting-state networks: an atlas-based MEG beamformer solution. Neuroimage 59, 3909-3921.

Himberg, J., Hyvarinen, A., 2003. ICASSO: Software for investigating the reliability of ICA estimates by clustering and visualization. 2003 Ieee Xiii Workshop on Neural Networks for Signal Processing - Nnsp'03, 259-268.

Hipp, J.F., Engel, A.K., Siegel, M., 2011. Oscillatory synchronization in large-scale cortical networks predicts perception. Neuron 69, 387-396.

Hipp, J.F., Hawellek, D.J., Corbetta, M., Siegel, M., Engel, A.K., 2012. Large-scale cortical correlation structure of spontaneous oscillatory activity. Nature Neuroscience 15, 884-890.

Holdefer, R.N., Sadleir, R., Russell, M.J., 2006. Predicted current densities in the brain during transcranial electrical stimulation. Clin Neurophysiol 117, 1388-1397.

Iacono, M.I., Neufeld, E., Akinnagbe, E., Bower, K., Wolf, J., Vogiatzis Oikonomidis, I., Sharma, D., Lloyd, B., Wilm, B.J., Wyss, M., Pruessmann, K.P., Jakab, A., Makris, N., Cohen, E.D., Kuster, N., Kainz, W., Angelone, L.M., 2015. MIDA: A Multimodal Imaging-Based Detailed Anatomical Model of the Human Head and Neck. PLoS One 10, e0124126.

Johnston, M.V., 2004. Clinical disorders of brain plasticity. Brain Dev 26, 73-80.

Lew, S., Wolters, C.H., Anwander, A., Makeig, S., MacLeod, R.S., 2009. Improved EEG Source Analysis Using Low-Resolution Conductivity Estimation in a Four-Compartment Finite Element Head Model. Human Brain Mapping 30, 2862-2878.

Li, Y.O., Adali, T., Calhoun, V.D., 2007. Estimating the number of independent components for functional magnetic resonance imaging data. Human Brain Mapping 28, 1251-1266.

Liu, Q., Balsters, J.H., Baechinger, M., van der Groen, O., Wenderoth, N., Mantini, D., 2015. Estimating a neutral reference for electroencephalographic recordings: the importance of using a high-density montage and a realistic head model. Journal of Neural Engineering 12, 056012.

Mantini, D., Corbetta, M., Perrucci, M.G., Romani, G.L., Del Gratta, C., 2009. Large-scale brain networks account for sustained and transient activity during target detection. Neuroimage 44, 265-274.

Mantini, D., Corbetta, M., Romani, G.L., Orban, G.A., Vanduffel, W., 2013. Evolutionarily novel functional networks in the human brain? Journal of Neuroscience 33, 3259-3275.

Mantini, D., Della Penna, S., Marzetti, L., de Pasquale, F., Pizzella, V., Corbetta, M., Romani, G.L., 2011. A signal-processing pipeline for magnetoencephalography resting-state networks. Brain Connect 1, 49-59.

Mantini, D., Franciotti, R., Romani, G.L., Pizzella, V., 2008. Improving MEG source localizations: an automated method for complete artifact removal based on independent component analysis. Neuroimage 40, 160-173.

Mantini, D., Perrucci, M.G., Cugini, S., Ferretti, A., Romani, G.L., Del Gratta, C., 2007a. Complete artifact removal for EEG recorded during continuous fMRI using independent component analysis. Neuroimage 34, 598-607.

Mantini, D., Perrucci, M.G., Del Gratta, C., Romani, G.L., Corbetta, M., 2007b. Electrophysiological signatures of resting state networks in the human brain. Proc Natl Acad Sci U S A 104, 13170-13175.

Marino, M.L., Q.; Brem, S.; Wenderoth, N.; Mantini, D., 2016. Automated detection and labeling of high-density EEG electrodes from structural MR images. Journal of Neural Engineering 13.

Mayhew, S.D., Hylands-White, N., Porcaro, C., Derbyshire, S.W., Bagshaw, A.P., 2013a. Intrinsic variability in the human response to pain is assembled from multiple, dynamic brain processes. Neuroimage 75, 68-78.

Mayhew, S.D., Ostwald, D., Porcaro, C., Bagshaw, A.P., 2013b. Spontaneous EEG alpha oscillation interacts with positive and negative BOLD responses in the visual-auditory cortices and default-mode network. Neuroimage 76, 362-372.

McKeown, M.J., Makeig, S., Brown, G.G., Jung, T.P., Kindermann, S.S., Bell, A.J., Sejnowski, T.J., 1998. Analysis of fMRI data by blind separation into independent spatial components. Human Brain Mapping 6, 160-188.

Michel, C.M., Murray, M.M., Lantz, G., Gonzalez, S., Spinelli, L., Grave de Peralta, R., 2004. EEG source imaging. Clin Neurophysiol 115, 2195-2222.

Ostwald, D., Porcaro, C., Bagshaw, A.P., 2010. An information theoretic approach to EEG-fMRI integration of visually evoked responses. Neuroimage 49, 498-516.

Ostwald, D., Porcaro, C., Bagshaw, A.P., 2011. Voxel-wise information theoretic EEG-fMRI feature integration. Neuroimage 55, 1270-1286.

Palva, J.M., Palva, S., 2012. Infra-slow fluctuations in electrophysiological recordings, blood-oxygenation-level-dependent signals, and psychophysical time series. Neuroimage 62, 2201-2211.

Pascual-Marqui, R.D., 2002. Standardized low-resolution brain electromagnetic tomography (sLORETA): Technical details. Methods and Findings in Experimental and Clinical Pharmacology 24, 5-12.

Pascual-Marqui, R.D., Lehmann, D., Koukkou, M., Kochi, K., Anderer, P., Saletu, B., Tanaka, H., Hirata, K., John, E.R., Prichep, L., Biscay-Lirio, R., Kinoshita, T., 2011. Assessing interactions in the brain with exact low-resolution electromagnetic tomography. Philos Trans A Math Phys Eng Sci 369, 3768-3784.

Pfurtscheller, G., Lopes da Silva, F.H., 1999. Event-related EEG/MEG synchronization and desynchronization: basic principles. Clin.Neurophysiol. 110, 1842-1857.

Porcaro, C., Ostwald, D., Bagshaw, A.P., 2010. Functional source separation improves the quality of single trial visual evoked potentials recorded during concurrent EEG-fMRI. Neuroimage 50, 112-123.

Ramon, C., Schimpf, P.H., Haueisen, J., 2006. Influence of head models on EEG simulations and inverse source localizations. Biomed Eng Online 5, 10.

Russell, G.S., Jeffrey Eriksen, K., Poolman, P., Luu, P., Tucker, D.M., 2005. Geodesic photogrammetry for localizing sensor positions in dense-array EEG. Clin Neurophysiol 116, 1130-1140.

Slutzky, M.W., Jordan, L.R., Krieg, T., Chen, M., Mogul, D.J., Miller, L.E., 2010. Optimal spacing of surface electrode arrays for brain-machine interface applications. Journal of Neural Engineering 7, 26004.

Smit, D.J., Stam, C.J., Posthuma, D., Boomsma, D.I., de Geus, E.J., 2008. Heritability of "small-world" networks in the brain: a graph theoretical analysis of resting-state EEG functional connectivity. Human Brain Mapping 29, 1368-1378.

Smith, S.M., Nichols, T.E., 2009. Threshold-free cluster enhancement: addressing problems of smoothing, threshold dependence and localisation in cluster inference. Neuroimage 44, 83-98.

Song, J., Davey, C., Poulsen, C., Luu, P., Turovets, S., Anderson, E., Li, K., Tucker, D., 2015. EEG source localization: Sensor density and head surface coverage. J Neurosci Methods 256, 9-21.

Van Hoey, G., Vanrumste, B., D'Have, M., Van de Walle, R., Lemahieu, I., Boon, P., 2000. Influence of measurement noise and electrode mislocalisation on EEG dipole-source localisation. Med Biol Eng Comput 38, 287-296.

Van Uitert, R., Weinstein, D., Johnson, C., 2003. Volume currents in forward and inverse magnetoencephalographic simulations using realistic head models. Ann Biomed Eng 31, 21-31.

VanVeen, B.D., vanDrongelen, W., Yuchtman, M., Suzuki, A., 1997. Localization of brain electrical activity via linearly constrained minimum variance spatial filtering. Ieee Transactions on Biomedical Engineering 44, 867-880.

Varela, F., Lachaux, J.P., Rodriguez, E., Martinerie, J., 2001. The brainweb: phase synchronization and large-scale integration. Nat.Rev.Neurosci. 2, 229-239.

Wagner, S., Rampersad, S.M., Aydin, U., Vorwerk, J., Oostendorp, T.F., Neuling, T., Herrmann, C.S., Stegeman, D.F., Wolters, C.H., 2014. Investigation of tDCS volume conduction effects in a highly realistic head model. Journal of Neural Engineering 11, 016002.

Wang, J.Z., Williamson, S.J., Kaufman, L., 1992. Magnetic Source Images Determined by a Lead-Field Analysis - the Unique Minimum-Norm Least-Squares Estimation. Ieee Transactions on Biomedical Engineering 39, 665-675.

Wang, Y.H., Gotman, J., 2001. The influence of electrode location errors on EEG dipole source localization with a realistic head model. Clinical Neurophysiology 112, 1777-1780.

Wolters, C.H., Anwander, A., Tricoche, X., Weinstein, D., Koch, M.A., MacLeod, R.S., 2006. Influence of tissue conductivity anisotropy on EEG/MEG field and return current computation in a realistic head model: a simulation and visualization study using high-resolution finite element modeling. Neuroimage 30, 813-826.

Wolters, C.H., Grasedyck, L., Hackbusch, W., 2004. Efficient computation of lead field bases and influence matrix for the FEM-based EEG and MEG inverse problem. Inverse Problems 20, 1099-1116.

Yuan, H., Ding, L., Zhu, M., Zotev, V., Phillips, R., Bodurka, J., 2016. Reconstructing Large-Scale Brain Resting-State Networks from High-Resolution EEG: Spatial and Temporal Comparisons with fMRI. Brain Connect 6, 122-135.